

Understanding and Mitigating Oxidation-Induced Electrical Instability in Sputtered Sc Thin Films

Jeonho Kim,¹ Indira Kiladze,¹ Clement Porret,¹ Bert Pollefliet,¹ and Johan Swerts¹
Imec, Kapeldreef 75, 3001 Leuven, Belgium

(*Electronic mail: johan.swerts@imec.be)

(Dated: 28 November 2025)

Scandium (Sc) thin films are promising candidates for advanced electronic applications due to their excellent electrical and thermal properties. However, the reliability is challenged by oxidation-induced instability. This study identifies and decouples two distinct oxidation mechanisms: transient oxidation during the deposition phase, driven by residual oxygen at plasma ignition, and ambient-induced oxidation post-deposition. Sequential wafer analysis reveals a pronounced first-wafer effect, with elevated sheet resistance (R_s) and non-uniformity (NU%) in early wafers. Grazing incidence X-ray diffraction (GI-XRD) and long-term statistical process control (SPC) confirm surface oxidation and its temporal evolution. An in-situ 5 nm Ru capping layer effectively suppresses ambient oxidation, stabilizing R_s , though NU% remains high due to deposition variability. These findings highlight the importance of both surface passivation and precise process control to ensure the electrical stability of Sc thin films.

I. INTRODUCTION

Scandium-based thin films have attracted significant interest as promising materials for microelectronic and energy device applications because of unique combination of low electrical resistivity, high thermal stability, and compatibility with next-generation material systems¹. Recent studies have further highlighted the potential in advanced interconnects and thin-film transistor technologies, particularly in the context of electrical reliability and integration feasibility^{2,3}. Extensive research has investigated Sc and its alloys as interconnect materials, highlighting their excellent current-carrying capabilities and strong resistance to electromigration⁴. Furthermore, the incorporation of Sc has been shown to modulate the electronic and ionic behavior of complex oxides, such as Fe_2O_3 in sodium ion battery anodes⁵ and solution-processed InZnO semiconductors, where it suppresses carrier density by tuning defect energetics⁶. Sc-based compounds have also demonstrated functional versatility in gate dielectric applications, as exemplified by water-induced Sc_2O_3 layers that allow low operating voltage metal oxide n- and p-type thin-film transistors⁷. Despite these attractive properties, the practical deployment of elemental Sc thin films remains hindered by pronounced reactivity with the environment⁸. Oxidation upon exposure to ambient conditions can significantly degrade the electrical performance of the capacitors, which presents challenges to the long-term stability of the device⁹. Thus, gaining a deeper understanding of electrical stability under realistic operational conditions is critical to unlocking the full technological potential. Previous studies have reported that Sc readily oxidizes upon exposure to ambient conditions, leading to resistivity degradation. For instance, research on scandium nitride (ScN) thin films has shown that oxidation impairs electrical properties, resulting in increased resistivity¹⁰. Although extensive research has been conducted on the oxidation behavior of bulk Sc, relatively few studies have focused on the oxidation effects in thin films¹¹. Recent reports suggest that the oxidation of transition metal thin films can significantly affect electrical

properties, with oxygen incorporation leading to increased resistivity and defect formation¹². Building on this, our study aims to explore the oxidation behavior of sputtered Sc thin films and its correlation with electrical instability. Unlike previous bulk material studies, we focus on oxidation at the thin-film level and its influence on crystallinity and electrical transport properties. Our findings provide insights into the importance of deposition conditions in controlling variations in oxidation-driven resistivity.

II. EXPERIMENTAL

Scandium (Sc) thin films were deposited using physical vapor deposition (PVD). The target material was 100% scandium with a purity of 2N5, supplied by a commercial vendor. Pre-sputtering and dummy wafer processing were performed with the Sc target prior to each deposition cycle to condition the chamber and target surface. The deposition chamber was typically maintained within a base pressure range of 1×10^{-9} to 5×10^{-9} Torr to minimize residual oxygen and moisture prior to plasma ignition. Depositions were performed on 100 nm- SiO_2 /p-Si wafers (300 mm) without external wafer heating under ambient-temperature conditions, using a Canon Anelva C-7100GT PVD system equipped with DC magnetron cathodes for metal deposition. Throughout the entire process, all wafers were either inside semiconductor processing equipment or measurement tools, or otherwise stored exclusively in SEMI-standard FOUPs (Front Opening Unified Pods). This protocol ensured that wafer handling and storage met industry standards for contamination control, and the results represent the behavior of thin films under conditions highly relevant to industrial applications. Post-deposition sheet resistance (R_s) was measured at 49 points in each wafer using a four-point probe mapping system. Film density was calculated by measuring the mass of the deposited Sc thin films using a wafer weighing system. The mass was determined by comparing the weight of the wafer before and

after deposition. Thickness and crystallinity were analyzed using X-ray reflectivity (XRR) and X-ray diffraction (XRD) techniques. XRD was conducted with a 2Theta-Omega scanning axis to assess bulk crystallinity, while grazing incidence X-ray diffraction (GI-XRD) was employed to examine near-surface characteristics with a fixed incident angle. This setup difference enabled a more comprehensive evaluation of Sc thin films, effectively distinguishing bulk crystallinity from surface oxidation effects.

III. RESULTS AND DISCUSSION

A. First wafer effect

A consecutive deposition experiment was performed to examine wafer-to-wafer trends in R_s . As shown in Figure 1, R_s measurements taken immediately after deposition revealed a systematic trend: The first wafer exhibited the highest R_s value (67.3 Ω/\square), while subsequent wafers demonstrated progressively lower R_s values. To confirm thickness consistency, X-ray Reflectivity (XRR) measurements were conducted at five radial positions (0, 35, 70, 105, and 140 mm) on each wafer. The average of these five points was used as the representative thickness per wafer. The XRR results confirmed that the film thickness remained nearly constant across all wafers, indicating that the observed variation in R_s cannot be attributed to non-uniform thickness. To further evaluate whether this variation stems from differences in intrinsic film quality, the resistivity of each wafer was calculated using the measured R_s and corresponding XRR thickness values. As summarized in Table I, resistivity consistently decreased from 223.2 to 184.9 $\mu\Omega\cdot\text{cm}$ over the six wafers, mirroring the R_s trend. This suggests that the elevated R_s in the first wafer is not merely a surface artifact but reflects degraded bulk electrical properties as well. Although sequential wafer processing may result in a slight increase in wafer temperature due to plasma irradiation, our PVD system is equipped with water cooling for both the substrate holder and cathodes, effectively minimizing this effect. As a result, any temperature rise during deposition is expected to be minor.

Additional evidence supporting this interpretation is provided in Figure 2, which shows a negative correlation between chamber idle time and R_s . As idle time increases prior to deposition, R_s values systematically decrease, suggesting that longer idle periods allow more complete evacuation of residual oxygen and moisture from the chamber. This supports the hypothesis that transient oxidation during initial plasma ignition contributes significantly to early-stage electrical instability in Sc thin films. Given that plasma ignition occurs at the bottom of the film rather than at the surface, the data indicate that early-stage instability is more likely driven by interfacial effects or structural imperfections than by surface oxidation. While the inverse relationship between idle time and residual oxygen is expected in vacuum systems, the pronounced sensitivity observed here suggests that Sc thin films are particularly susceptible to even trace amounts of reactive

TABLE I. Averaged R_s , XRR thickness, and resistivity values for six scandium wafers deposited under identical conditions.

	R_s (Ω/\square) ^a	XRR (nm) ^b	Resistivity ($\mu\Omega\cdot\text{cm}$) ^c	Density (g/cm^3) ^d
1st	67.29	33.17	223.19	2.89
2nd	64.36	33.10	213.02	3.04
3rd	62.37	33.12	206.59	3.02
4th	61.55	33.11	203.83	3.01
5th	59.85	33.09	198.04	2.98
6th	55.95	33.05	184.92	2.98

^a R_s measured by 4-point probe at 49 points; average reported.

^b XRR thickness from 5-point radius scan; average reported.

^c Resistivity calculated from average R_s and thickness.

^d Calculated from measured wafer mass and XRR thickness.

species during nucleation. The presence of residual oxygen may have influenced nucleation dynamics or defect formation at the Sc/SiO₂ interface, thereby degrading electrical performance. This interpretation is further supported by density measurements, which show that the first wafer has the lowest value (2.89 g/cm^3), while subsequent wafers range between 2.98 and 3.04 g/cm^3 without a consistent trend. The distinctly lower density in the first wafer suggests incomplete nucleation or increased porosity, which can degrade electrical performance independently of oxidation. Based on the data, a plausible explanation is the first wafer experienced greater residual oxygen or moisture exposure in the chamber at the onset of deposition. However, since plasma ignition occurs at the bottom of the film, not at the surface, the resulting instability is more likely due to interfacial reactions or structural imperfections—such as increased defect density or porosity—rather than localized surface oxidation. These early-stage conditions may have disrupted uniform nucleation and grain growth at the Sc/SiO₂ interface, contributing to the elevated R_s observed in the first wafer.

Figure 3 further illustrates the R_s distribution of scandium (Sc) thin films deposited sequentially on six wafers, based on 49-point R_s measurements per wafer. A clear decreasing trend in both the average and median R_s values is observed from the first to the sixth wafer. Along with the drop in mean R_s , the non-uniformity—defined by the inter-quartile range and the presence of outliers—also decreases as the deposition sequence progresses. The first wafer displays the widest R_s distribution and the highest overall values, whereas the sixth wafer shows the lowest resistance and the narrowest spread. This observation suggests that the increased R_s in the first wafer is likely caused by insufficient conditioning due to residual moisture in the chamber during initial plasma ignition. Even with standard pre-sputtering procedures, the first plasma ignition may induce transient oxygen release, leading to surface oxidation at the early deposition stage. The presence of reactive oxygen species could contribute to the initial formation of oxide or the incorporation of defects, negatively affecting the film quality. The interaction of Sc with oxygen species on the SiO₂/Si substrate, particularly in the first wafer, likely results in interfacial oxide layers that hinder uniform grain growth and increase R_s . This finding highlights the crit-

This is the author's peer reviewed, accepted manuscript. However, the online version of record will be different from this version once it has been copyedited and typeset.
PLEASE CITE THIS ARTICLE AS DOI: 10.1116/6.0004952

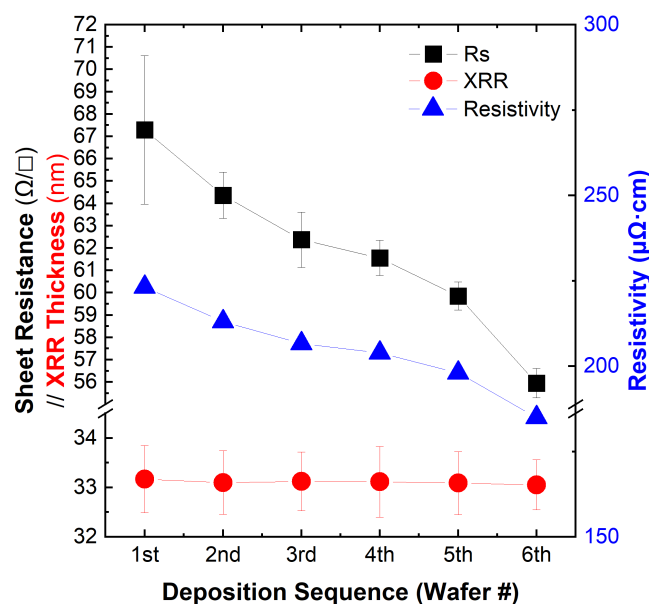


FIG. 1. Variation of sheet resistance (R_s), thickness, and calculated resistivity across six consecutively deposited Sc thin films. A clear decreasing trend is observed, indicating a first-wafer effect.

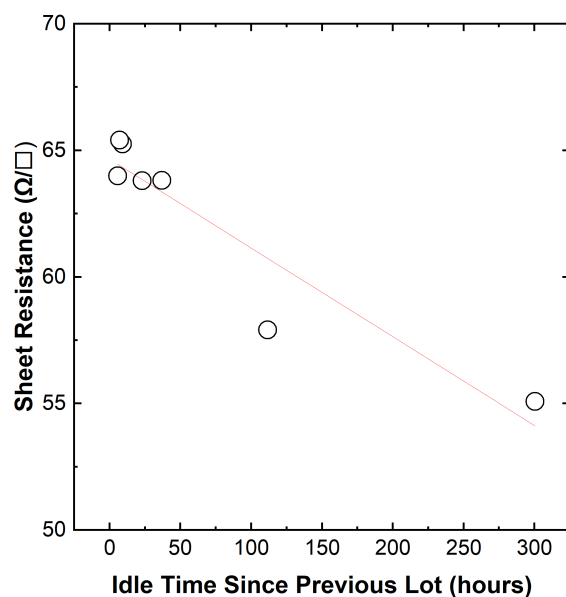


FIG. 2. Correlation between chamber idle time and R_s . Longer idle times result in lower R_s , supporting the hypothesis that residual oxygen contributes to early-stage oxidation.

ical role of initial deposition conditions in achieving stable and high-quality Sc thin films.

B. Time-Dependent Aging and Oxidation

To evaluate sheet resistance stability over time, periodic post-deposition R_s measurements were conducted. As shown

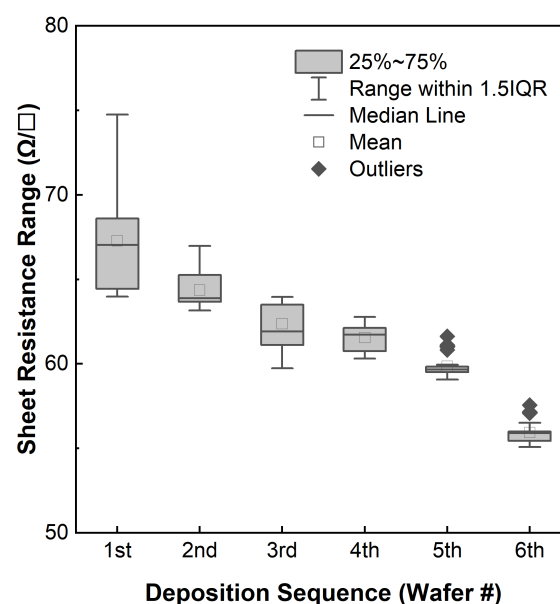


FIG. 3. Box plots of R_s distribution across six wafers. The first wafer shows the widest spread and highest R_s , while subsequent wafers show improved uniformity and lower resistance.

in Figure 4, R_s exhibited a gradual increase across all wafers, irrespective of their initial values, suggesting a progressive oxidation mechanism upon air exposure. Given scandium's strong affinity for oxygen, the R_s increase likely follows a two-stage oxidation process, as described by Grömbel et al.¹³:

(1) Initial surface-limited oxidation - formation of a thin ScO or Sc_2O_3 layer at the film-air interface, reducing carrier mobility;

(2) Grain boundary diffusion - oxygen penetration into deeper regions of the film, progressively degrading bulk conductivity.

While the observed resistivity increase strongly suggests oxidation-driven aging, the lack of direct chemical and depth-profile analyses precludes definitive identification of the dominant oxidation mechanism. The present interpretation is based on electrical and structural trends, which provide strong indications but do not fully resolve the relative contributions of surface-limited and bulk oxidation pathways. Further mechanistic insight would benefit from advanced compositional and depth-profiling techniques, such as XPS or SIMS, which could clarify the nature and extent of oxidation processes in Sc thin films. This study was designed to focus on structural and electrical stability under fab-realistic conditions, while a detailed chemical analysis of surface oxidation is reserved for future research.

C. Crystallinity and Film Properties

X-ray diffraction (XRD) analysis was conducted to assess the bulk crystallinity of the deposited Sc thin films. As shown in Figure 5, all six wafers exhibited a dominant Sc (002) ori-

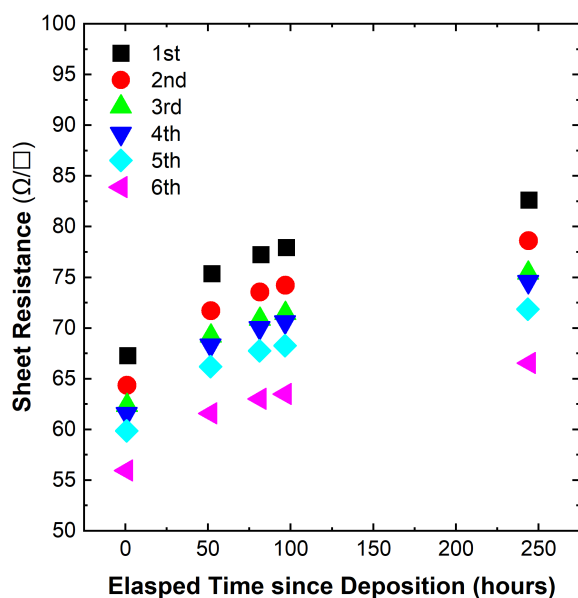


FIG. 4. Time-dependent R_s measurements for six wafers. All wafers exhibit gradual R_s increase over time, suggesting progressive oxidation upon ambient exposure.

entation peak, confirming a consistent out-of-plane texture in the films. No secondary peaks corresponding to Sc_2O_3 were detected in the XRD spectra, indicating that bulk crystallinity is preserved and any oxidation effects—if present—are likely surface-confined or amorphous in nature. To further investigate near-surface structural changes, grazing incidence X-ray diffraction (GI-XRD) was employed. Figure 6 presents the GI-XRD spectra across all wafers, where the first wafer shows faint features near 30.8° and adjacent positions. These peaks were initially attributed to crystalline Sc oxides (ScO and Sc_2O_3), but given the overlap with Sc's intrinsic reflections and the enhanced surface sensitivity of GI-XRD, their origin remains inconclusive. The absence of these features in standard XRD supports the interpretation that they are surface-related. A closer look at the region surrounding the Sc (002) peak is provided in Figure 7. The first wafer shows a slight shift in the Sc (002) peak position, along with two minor peaks near the Sc (100) reflection that are not present in other wafers. These additional peaks are located close to the expected positions of ScO (200) and Sc_2O_3 (211), raising the possibility of oxidation-related phases. In particular, GI-XRD's asymmetric geometry enhances surface sensitivity and can amplify weak Sc peaks that are not visible in standard 2θ - θ XRD, potentially leading to misinterpretation. Given that crystallization of Sc oxides at room temperature is rarely reported in literature¹¹, and considering the sharpness and consistency of the observed peaks, it is plausible that these features reflect Sc-related structural transitions rather than definitive oxide formation. This interpretation is consistent with the expectation that any ScO formed during deposition would be limited in thickness and therefore produce broad, less-defined diffraction features. Such behavior has also been reported

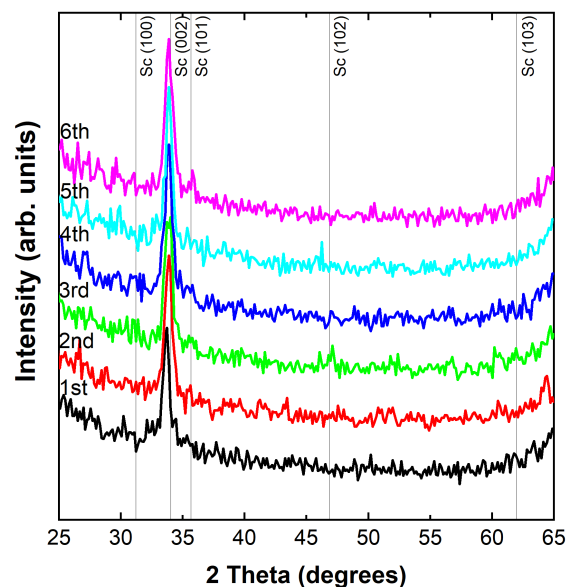


FIG. 5. XRD patterns of Sc thin films showing dominant Sc (002) orientation with no detectable oxide peaks, indicating bulk crystallinity is preserved.

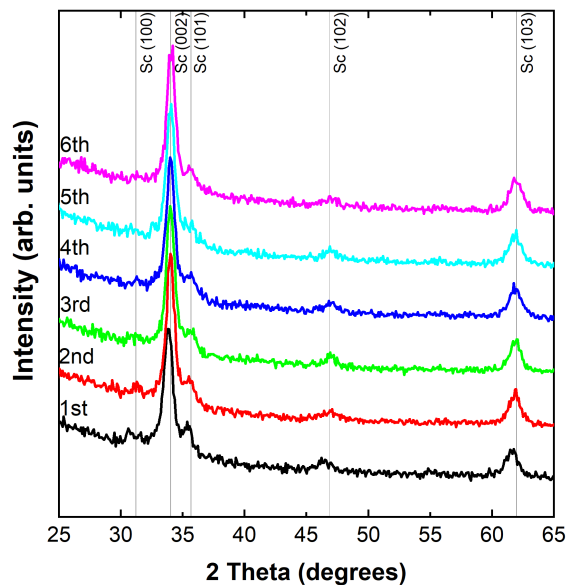


FIG. 6. GI-XRD spectra of the first wafer showing faint scandium oxide peaks, potentially overlapping with Sc reflections and suggesting surface-related structural changes.

in previous studies on oxidation-related defects, which have been shown to adversely affect the electrical properties of thin films¹⁴.

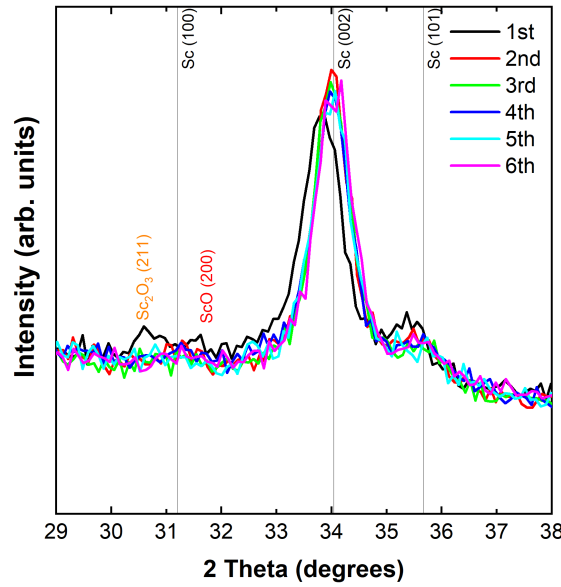


FIG. 7. Peak shifts in Sc (002) and additional features near Sc (100) in the first wafer, possibly related to oxidation or structural variations.

D. Decoupling Oxidation Effects via In-Situ Ru Capping Layer

To mitigate the oxidation-induced instability observed in Sc thin films, a 5 nm Ru capping layer was implemented in-situ on top of the Sc layer prior to exposure to ambient conditions. Ru was chosen as a representative industry-standard capping metal to demonstrate the passivation concept, consistent with the prior use of Ru caps in thin film stacks and its barrier functionality^{15,16}. Figure 8 presents a comparative analysis of the sheet resistance data in the form of box plots, clearly demonstrating the stabilizing effect of the capping layer. Ru-capped Sc films exhibit significantly improved electrical stability, with R_s values consistently ranging between 36.3 and 38.7 Ω/\square over a 378-day monitoring period. In contrast, uncapped Sc films showed a larger variation, from 51.9 to 64.7 Ω/\square over a 303-day period. The wafer-to-wafer non-uniformity percentage (WtWNU %) was also markedly reduced, from 4.69 % in uncapped Sc films to 2.15% in capped ones. The consistently low R_s values observed for extended periods, even after a prolonged idle time of the chamber, suggest that the Ru capping layer primarily functions as an effective diffusion barrier against oxidation rather than contributing significantly to electrical conduction. This interpretation is supported by the fact that standalone 5 nm Ru films typically exhibit sheet resistance values around 80 Ω/\square , with non-uniformity (WiWNU%) consistently below 1.0%. Interestingly, the Ru/Sc bilayer structure yields R_s values as low as 35 Ω/\square , which is significantly lower than the standalone Ru or Sc layers. This phenomenon can be explained by a combination of factors: (1) a parallel conduction model, where both Ru and Sc layers contribute to current

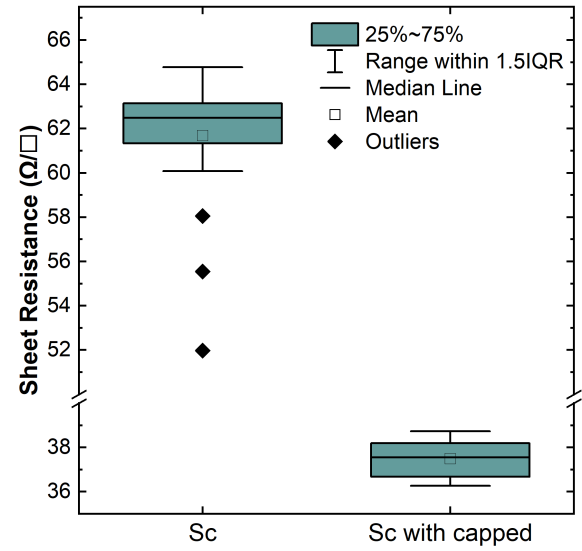


FIG. 8. Box plot comparison of R_s in Ru-capped vs. uncapped Sc films. Ru capping significantly stabilizes R_s over 378 days.

flow; (2) improved surface morphology due to Ru capping, which reduces roughness and enhances carrier mobility; and (3) favorable interfacial effects that facilitate more efficient electron transport. These synergistic effects highlight the complex interplay between material interfaces and electrical performance in bi-layer thin films. In Figure 9, WiWNU% is plotted against the Statistical Process Control (SPC) monitoring sequence, where each point represents a new wafer deposited and measured biweekly under identical conditions. While R_s values remain stable in capped samples, NU% shows persistent variation, indicating that non-uniformity (WiWNU%) arises primarily from deposition-phase instability. Figure 10 plots NU% against R_s mean, revealing no direct correlation between the two metrics. This decoupling strongly supports the hypothesis that NU% is governed by deposition-phase variability, whereas R_s mean is primarily affected by post-deposition oxidation. These results highlight the need for further optimization of plasma ignition and chamber conditioning to improve uniformity, in addition to employing surface passivation strategies. While the Ru capping layer effectively suppresses surface oxidation, it does not inhibit oxidation at the Sc/SiO₂ interface, which originates during the early stages of deposition. This interface oxidation, unaffected by post-deposition passivation, remains a critical challenge in achieving fully stable Sc thin films.

IV. SUMMARY AND CONCLUSIONS

This work provides a comprehensive understanding of oxidation-induced electrical instability in sputtered Sc thin films by distinguishing between deposition-phase and

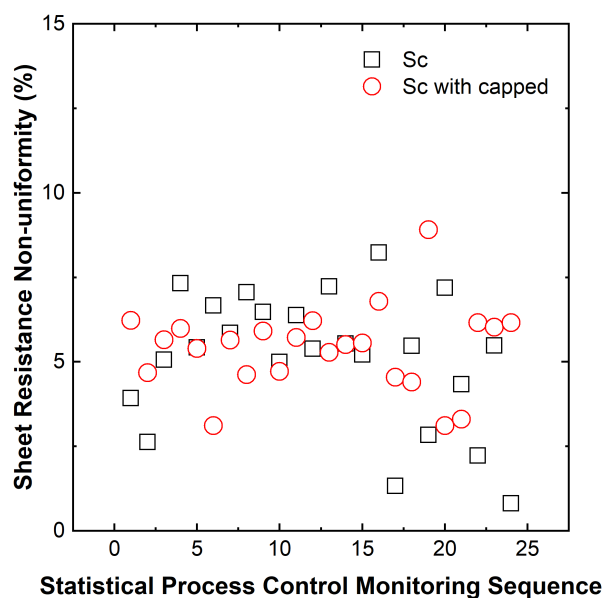


FIG. 9. WiWNU% plotted over SPC monitoring sequence, showing persistent non-uniformity due to deposition variability.

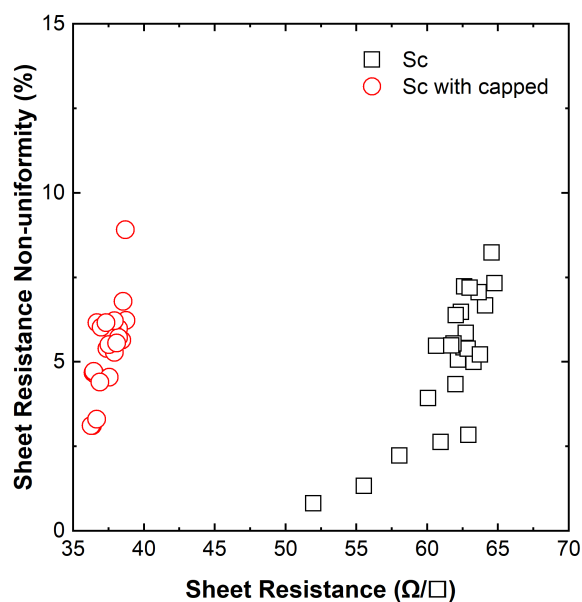


FIG. 10. WiWNU% vs. R_s mean. The lack of correlation supports the decoupling of deposition-phase and post-deposition oxidation effects.

ambient-phase oxidation mechanisms. The first-wafer effect and chamber idle time correlation highlight the critical role of transient oxidation during plasma ignition. Meanwhile, ambient exposure leads to progressive R_s degradation, confirmed by GI-XRD and SPC monitoring. Although Ru capping effectively mitigates ambient oxidation, deposition-phase variability continues to affect NU%. Therefore, ensuring long-term reliability of Sc thin films requires a dual strategy that involves implementing robust surface passivation as well as

optimizing deposition conditions to minimize transient oxidation during deposition onset and uniformity issues. In particular, the adoption of pre-deposition wafer treatments, such as in-situ degas or plasma to remove moisture and native oxides, together with extending the duration of target pre-sputtering on dummy wafers, can be considered effective approaches to further suppress transient oxidation and reduce the first-wafer effect.

ACKNOWLEDGMENTS

We gratefully acknowledge the support of the imec core program members, the European Commission, local authorities, the imec pilot line, the imec material characterization and analysis group, and the imec Fab Engineering.

AUTHOR DECLARATIONS

Conflict of interest

The authors have no conflicts to disclose.

DATA AVAILABILITY STATEMENT

The data that support the findings of this study are available within the article.

- ¹G. B. Rayner, N. O. Jr., B. Liu, J. Shallenberger, J. Zhu, T. Palacios, P. Behera, S. Cheema, B. Johs, and N. A. Strnad, *J. Vac. Sci. Technol. A* **43**, 020401 (2025).
- ²C. Porret, J.-L. Everaert, M. Schaekers, L.-A. Ragnarsson, A. Hikavyy, E. Rosseel, G. Rengo, R. Loo, R. Khazaka, M. Givens, X. Piao, S. Mertens, N. Heylen, H. Mertens, C. T. De Carvalho Cavalcante, G. Sterckx, S. Brus, A. N. Mehta, M. Korytov, D. Batuk, P. Favia, R. Langer, G. Pourtois, J. Swerts, E. D. Litta, and N. Horiguchi, 2022 International Electron Devices Meeting (IEDM), 34.1.1–34.1.4 (2022).
- ³B. Pollefliet, C. Porret, J.-L. Everaert, K. Sankaran, X. Piao, E. Rosseel, T. Conard, A. Impagnatiello, Y. Shimura, N. Horiguchi, R. Loo, A. Vantomme, and C. Merckling, *Japanese Journal of Applied Physics* **63**, 02SP97 (2024).
- ⁴Y. Yang, S. Xu, S. Xie, and L.-M. Peng, *Nano-Micro Lett.* **2**, 184–189 (2010).
- ⁵D. Nayak, S. Puravankar, S. Ghosh, and V. Adyam, *Nano-Micro Lett.* **25**, 5857–5868 (2019).
- ⁶Y. Choi, G. H. Kim, W. H. Jeong, J. H. Bae, H. J. Kim, J.-M. Hong, and J.-W. Yu, *Appl. Phys. Lett.* **97**, 162102 (2010).
- ⁷A. Liu, G. Liu, H. Zhu, H. Song, B. Shin, E. Fortunato, R. Martins, and F. Shan, *Adv. Funct. Mater.* **25**, 7180–7188 (2015).
- ⁸A. Shih, J. Yater, C. Hor, and R. Abrams, *Appl. Surf. Sci.* **211**, 136–145 (2003).
- ⁹S. Choudhary, J. V. N. Sarma, S. Pande, S. Ababou-Girard, P. Turban, B. Lepine, and S. Gangopadhyay, *AIP Advances* **8**, 055114 (2018).
- ¹⁰S. Cichoń, J. More-Chevalier, U. D. Wdowik, E. de Prado, J. Bulíř, M. Novotný, L. Fekete, J. Duchoń, and J. Lančok, *Appl. Surf. Sci.* **674**, 160867 (2024).
- ¹¹R. Coloma Ribera, R. W. E. van de Kruijs, A. E. Yakshin, and F. Bijkerk, *J. Appl. Phys.* **118**, 055303 (2015).
- ¹²C. R. S. V. Boas, J. M. Sturm, and F. Bijkerk, *J. Appl. Phys.* **126**, 155301 (2019).



This is the author's peer reviewed, accepted manuscript. However, the online version of record will be different from this version once it has been copyedited and typeset.

PLEASE CITE THIS ARTICLE AS DOI: 10.1116/6.0004952

- ¹³J. Grümbel, J. Bläsing, F. Hörich, A. Dadgar, R. Goldhahn, and M. Feneberg, *J. Appl. Phys.* **137**, 145703 (2025).
¹⁴M. Li, H. Lin, and K. H. Y. Zhu, *Appl. Phys. Lett.* **121**, 111602 (2022).

- ¹⁵S.-H. Hsieh, W. J. Chen, and C.-M. Chien, *Nanomaterials* **5**, 1840–1852 (2015).
¹⁶P. yang Yan, E. Spiller, and P. Mirkarimi, *J. Vac. Sci. Technol. B* **25**, 1859–1866 (2007).